Synthesis and Characterization of $Ba_{0.8}Sr_{0.2}Ce_{1-x}Zr_xY_{0.1}O_{3-\delta}$ Proton-Conducting Electrolyte for Solid Oxide Fuel Cell

J. Madhuri Sailaja[1], V. Veeraiah[2]
[1]*Dept of Physics, AUCEW, Andhra University, Vishakhapatnam*

Abstract **- Proton conducting oxides $Ba_{0.8}Sr_{0.2}Ce_{0.9-x}Zr_xY_{0.1}O_{3-\delta}$ $(0\leq x\leq 0.2)$ are prepared using the citrate-EDTA complexing sol-gel method. The effect of zirconium doping on the material properties are systematically investigated. The phase, Thermal analysis, Morphology, chemical Stability and Conductivity measurements are performed on the sintered powders through TGDTA, XRD, SEM, EDAX, FTIR, RAMAN and LCR measurements. The results indicated that a single phase Orthorhombic system. Zirconium doping helped in increasing the grain size while reducing the lattice parameters and unit cell volume. The ionic conductivities of the $Ba_{0.8}Sr_{0.2}Ce_{0.9-x}Zr_xY_{0.1}O_{3-\delta}$ sintered oxides increased with increase in the concentration of Zr Among the synthesized samples of $Ba_{0.8}Sr_{0.2}Ce_{0.7}Zr_{0.2}Y_{0.5}O_{3-\delta}$ pellet showed the highest conductivity with a value of $2.05x10^{-3}$S/cm at 500°C due to its smaller lattice volume, larger grain size and lower activation energy. All pellets exhibited good chemical stability when exposed to air and H_2o atmospheres. These results indicate that this composition can be used as a potential electrolyte if synthesis conditions and temperature are well maintained.**

Index Terms **- $Ba_{0.8}Sr_{0.2}Ce_{0.9-x}Zr_{0.2}Y_{0.1}O_{3-\delta}$, Chemical stability, Proton conducting electrolyte, Raman, Solid oxide Fuel Cell, Sol-Gel synthesis.**

INTRODUCTION

Increasing global demands on supply of fuels stimulate extensive investigations towards sustainable energy sources and more efficient energy converting methods. During the past decades, solid oxide fuel cells (SOFCs) with solid oxide ceramics as the electrolyte have a potential to convert the chemical energy from the fuel directly to electricity and gained attention as promising power generation systems due to their high thermodynamic efficiency, low environmental impact, fuel flexibility, ability to use non-precious-metal catalysts and green house-gas free energy in the fields of transportation and stationary applications. [1-3]. In particular, perovskite type oxides based on $SrCeO_3$ or $BaCeO_3$ when doped with some trivalent cations depict considerably high protonic conductivity when they are subjected to atmospheres like humidified hydrogen at temperatures >300°C [4, 5]. The present most favored SOFC electrolyte is yttrium doped with zirconium (YSZ) which creates oxygen ion vacancies thus promoting high conductivity with operating temperatures in the range 800°- 1000°C.Inspite many benefits of having like high temperature operation , fuel flexibility, availability of electrode materials at a lesser cost, efficient cogeneration capabilities, such high temperatures can lead to material degradation, reactions between the components, sealing and a long start up and shutoff periods etc [6,7].

According to Zhang [8] substitution of an element with higher ionic size when compared to Ce increases the protonic conductivity of Yttrium doped $BaCeO_3$ while dopant with higher electro negativity enhances their chemical stability. Thus new compounds exhibiting high conductivity at low temperatures are in search which resulted in the development of solid oxide fuel cells (IT SOFCs) in the range of intermediate temperature ranging between 400°-700°C.The key issue lies in the synthesis of a highly proton conductive electrolyte with improved chemical stability.

$BaCeO_3$ and $BaZrO_3$ can easily form a solid solution for all the composition range and it has been proved viable to replace a portion of Ce with Zr which hiked chemical stability due to decrease in the bond length M-O, with a corresponding change of e oxide's properties from basic to acidic that hinders the formation of carbonates, hydroxides etc. Co doping strategy has been successfully employed with trivalent ions like Y^{3+} which creates oxygen vacancies resulting in enhancing protonic conductivity of barium

Zirconate-Cerate solution [8, 9]. Another challenging issue in Y doped $BaCeO_3$ electrolytes for H^+-SOFC applications is thermal instability due to reaction of cations with C_O^{2-}, H_2O or H_2S- containing atmospheres [10-12].Thermodynamically the chemical stability of $SrCeO_3$ is greater than $BaCeO_3$[13]. The consequences of A site doping on the stability and conductivity issues have been less reported. Therefore Sr can be partially substituted into the perovskite structure replacing barium in the A sites while cerium is partially replaced with Zr and Y on the B site in the present study. Sheng -Wei Lee et al. has worked on the effect of strontium with the composition $Ba_{1-x}Sr_xCe_{0.6}Zr_{0.2}Y_{0.2}$ ($0\leq x\leq 1$) and reported good chemical stability to CO_2 containing atmospheres [13].

Several synthesis techniques like Mechanical Ball milling method of solid state reaction [14], Hydro thermal reaction [15], Auto combustion [16] and Sol-gel [17] have been quoted in the literature. When compared with conventional solid state reaction method, wet chemistry methods gained the advantage that the constituent ions can be homogenously mixed at the atomic level in the solution which resulted in fine particles with appreciable sintering capability. $BaZr_{0.1}Ce_{0.7}Y_{0.2}O_{3-\delta}$ prepared by gel-casting technique reported better electrical conductivity and increased chemical stability than that of the same composition prepared by solid state method [18]. Accordingly $Ba_{0.8}Sr_{0.2}Ce_{0.9-x}Zr_xY_{0.1}O_{3-\square}$ (x=0.04,0.08, 0.16, 0.2) has been synthesized using citrate–ethylene diaminetetraacetic acid (EDTA) complexing sol-gel method and the effect of Zr doping on the micro structure and conductivity of $BaCeO_3$ perovskite proton conducting oxides is studied.

1.1. EXPERIMENTAL

A. POWDER PREPARATION

The citrate-EDTA complexing sol-gel process is adopted for preparing $Ba_{0.8}Sr_{0.2}Ce_{0.9-x}Zr_xY_{0.1}O_{3-\delta}$ (x=0.04, 0.08, 0.16, 0.2) oxides. Initial materials were commercial Ba $(NO_3)_2$, ZrO $(NO_3)_2.2H_2O$, $Ce(NO_3)_3$ $6H_2O$ (HighMedia,99.5%). The precursor solution uses both citric acid and EDTA as chelating agents. The ratio of molar solutions of citric acid: EDTA: Total metal cations content is set at 2:1:1. The pH value of the solution is adjusted to be ~ 6 using NH_4OH. The mixed solutions are heated at 100°C under continuous stirring using magnetic stirrer until obtaining viscous gels. On further heated to a temperature of 250°C overnight to evaporate residual water and organics, these gels gets converted into black powders. The prepared powders are then calcined at 1000°C for 12 h with a heating rate of 5°C/min. To obtain dense samples, the calcined powders were uniaxially pressed into cylindrical pellets at 5ton pressure for 5 min and then sintered in an air atmosphere. Sintering was carried out at 1300°C for 5 h at a heating rate of 5°C min^{-1}.

B. CHARACTERIZATION

Thermo gravimetric analysis (TGA) is carried out to the dried powder (T= 250°*C)* by a TA instrument (model SDT Q600). The phase identification of the sintered oxides is analyzed with a powder diffractometer (PANalytical X-pert Pro) with nickle filtered Cu Kα radiation and the diffraction angle from 10° to 90° with a step raise of 0.01°/min. The chemical stability of $Ba_{0.8}Sr_{0.2}Ce_{0.9-x}$ $Zr_xY_{0.1}O_{3-\delta}$ oxides are evaluated by exposing the sintered pellets to boiling water and CO_2 containing atmosphere. Microstructure of the sintered pellets are examined using Scanning Electron Microscope (JEOL model JSM-6610 LV) in conjunction with an Energy Dispersion Spectrometer (EDS) to estimate the percentage of elements present in the samples. A FTIR spectrometer (SHIMADZU IR Prestige-21, Singapore) is emused to record the Fourier transform infrared (FTIR) spectra of calcined and sintered $Ba_{0.8}Sr_{0.2}Ce_{0.9-x}$ $Zr_xY_{0.1}O_{3-\delta}$ powder in the range of 4,000 to 400 cm^{-1} to scrutnise the complex, carbonates and oxides formation. The theoretical density of the powders is manipulated with the obtained XRD. Fourier transforms Raman spectroscopy (BTC111- RAMAN-785) studies are conducted to study the Vibrational modes of the samples in the range 0-3000cm^{-1}. LCR measurements from room temperature to 400˚C are performed with Wayneker P65000 model in the frequency range from 20Hz to 1MHz after painting silver on both sides of the pellet and heating in a furnace at 375°C for 30min prior to the measurements. The crystallite sizes of the powder are measured using Scherrer's formula. The bulk densities of the sintered pellets are calculated with the help of Archimedes displacement method.

C. RESULTS AND DISCUSSIONS

Thermogravimetry/Differential thermal analysis.

To investigate the reaction during the formation of the perovskite phase structure, simultaneous TG-DTA curves of the samples are conducted from room temperature to 1200°C. Nitrates can be decomposed easily as they are less stable than carbonates. Three regions are represented in TG-DTA of the powder as shown in fig 1. The gradual weight loss is 5% up to 300˚C and is due to absorption of water molecules. The further weight loss followed by two exothermal peaks in DTA shows that the decomposition of gel takes place in two steps. The weight loss from 310˚C to 500˚C is found to be 12% accompanied with small exothermic peak at 418˚C which may be due to combustion of the metal nitrates. The weight loss from 500˚C -770˚C and the exothermic peak at 546˚ C is due to co-oxidation. A very small weight loss is observed above 900˚C may be due to thermal decomposition of barium carbonate, with the release of CO_2 [19,20] .There is no considerable weight change when the temperature is above 1000°C, indicating that complete decomposition of $BaCO_3$ and formation of $Ba_{0.8}Sr_{0.2}Ce_{0.9-x}Zr_xY_{0.1}O_{3-\delta}$ compound.

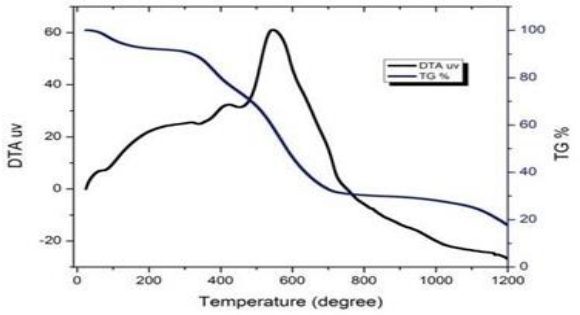

Fig. 1 TG-DTA curves of $Ba_{0.8}Sr_{0.2}Ce_{0.9-x}Zr_xY_{0.1}O_{3-\delta}$ powder preheated at 2500C for 24h.

XRD Analysis

Fig 2 reflects the XRD patterns of calcined and sintered ceramic powders. It is seen from TG- DTA measurements that the complete decomposition of carbonates/nitrates need 1000°C and correspondingly the XRD patterns at 1000°C confirm the single perovskite phase formation with very small $BaCeO_3$ and CeO_2 impurities. The formation of $BaCO_3$ impurity can be due to the reaction between Ba^{2+} ions and CO_3^{2-} ions which is the result of reaction between citric acid and EDTA in the process of heating [20]. In addition a small weak peak is observed in the calcined sample which may be attributed to CeO_2 like phase as the peaks are closer to the standard data JCPDF (33-0334) CeO. With the increase of Zr doping to 0.2 the CeO-like second phase is suppressed. Details of parameters regarding lattice and crystal structure are elucidated in the Table 1 given below.

All the sintered $Ba_{0.8}Sr_{0.2}Ce_{0.9-x}Zr_xY_{0.1}O_{3-\delta}$ oxides showed leading orthorhombic perovskite structure and the peaks matched with the characteristic diffraction pattern of $BaCeO_3$ (JCPDF 22-0074) showing seven diffraction peaks namely (002), (022), (213), (611), (422), (440), (613) planes. The lattice parameters are calculated from XRD analysis based on the standard data of $BaCeO_3$ and a linear relation between the lattice parameters and Sr doping content is noticed. Close examination of the XRD data discloses that as Zr is doped replacing some Ce in the B sites the diffraction peaks shifted to higher angles and decrease of the lattice parameters is observed, which shows a plane distance reduction (according to Bragg's law).This can be well elucidated by the fact that Zr^{4+} has a smaller ionic radius than Ce^{4+} and the correct doping and ordering of the atoms within the lattice reduces the strain. This results in the decrease in the cell volume which retains the structural stability against reactions with CO_2.

2(a)

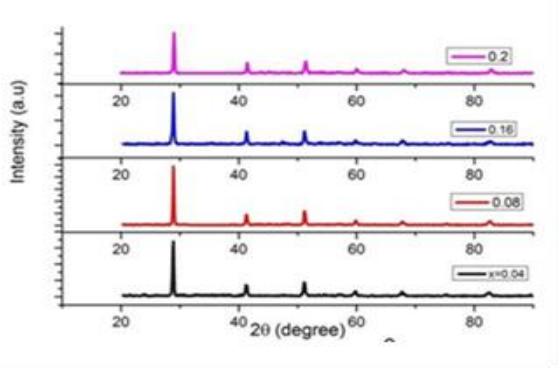

2(b)

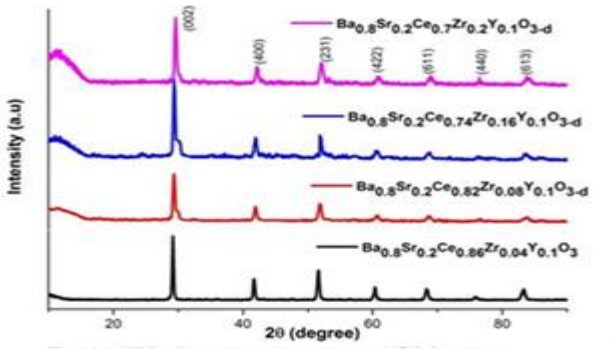

Sintered Samples

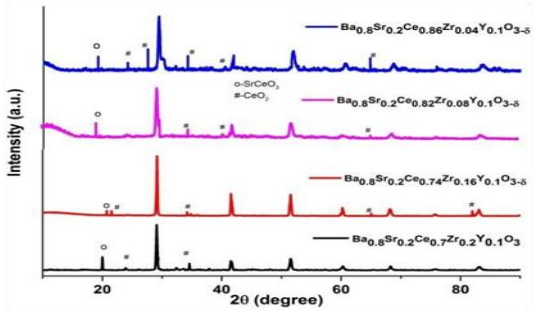

Fif2(c)

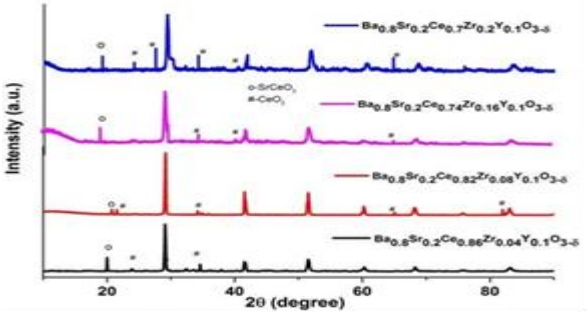

Fig 2(d)

Fig. 2 XRD patterns of (a) calcined (1000˚C) , (b)sintered (1300ºC), (c) exposed to boiling water and (d) exposed to CO_2 of $Ba_{0.8}Sr_{0.2}Ce_{0.9-x}ZxY_{0.1}O_3$ oxides

Table 1. Summary of Crystal parameters $Ba_{0.8}Sr_{0.2}Ce_{0.9-x}Zr_xY_{0.1}O_{3-\delta}$ powders

	Crystal Symmetry	a (Å)	b(Å)	c(Å)	Cell volume(Å)^3	Relative Density
BSCZY-1	Orthorhombic	8.672	6.147	6.113	323.93	85%
BSCZY-2	Orthorhombic	8.622	6.058	6.109	319.1	88%
BSCZY-3	Orthorhombic	8.722	6.076	6.012	318.91	88%
BSCZY-4	Orthorhombic	8.596	6.049	6.102	317.41	89%

Barium cerate structure is not chemically stable because it can react with CO_2 according to the reaction (3) or with H_2O according to reaction (4)

In order to verify the stability under H_2O containing atmospheres, the sintered pellets are boiled in water for 2hrs, dried and the XRD patterns are recorded. It has been observed that after exposed to boiling water, the $Ba_{0.8}Sr_{0.2}Ce_{0.9-x}Zr_xY_{0.1}O_{3-\delta}$ pellets retained original perovskite structure with less additional peaks showing $BaCO_3$ phase as shown in the Fig 2c. Due to reaction with H_2O, $BaCO_3$ might also be formed due to interaction with atmospheric CO_2 that converts Ba $(OH)_2$ into carbonate. The reaction biproduct CeO_2 that may appear is insoluble in water and forms a porous layer on the surface of the $BaCeO_3$ pellet while Ba $(OH)_2$ results in a significant volume expansion thereby forming cracks on the surface [21]. As a result water penetrates into the material through the cracks on the surface which resulted in the further reaction with $BaCeO_3$

$$BaCeO3 + CO2 \rightarrow BaCO3 + CeO2 \quad (3)$$

$$BaCeO3 + H2O \rightarrow Ba(OH)2 + CeO2 \quad (4)$$

Among the four compositions synthesized these peaks are less intense with Zr content of 0.2composition indicating its chemical stability in water while the composition x=0.04 recorded more impurity phase.

A neutron Diffraction study reveals that, at room temperature and pressure, in the replacement of Zr with Ce, the size of BO_6 octahedral decreases with rise in zirconium content as Zr acts as a phase stabilizer. Therefore the motive for the evolution towards a symmetric structure is increased and it becomes more difficult to distort structure of the perovskite. This also shows that stability in water increases with decreasing ionic radius of the codopant [12, 21, and 24] is decreased. To check the stability of the material against atmospheric CO_2 small amount is kept out in the laboratory for a period of 10 days and the XRD analysis did not report any phase change except for small peaks indicating $BaCO_3$. The slight split is observed in the XRD peak for x=0.16 composition which may be due to structural changes in the perovskite phase [13].These results suggested that when strontium is doped into barium cerates can definitely improve the chemical stability of $Ba_{0.8}Sr_{0.2}Ce_{0.9-x}Zr_xY_{0.1}O_{3-\delta}$ compound [12] and this is in agreement with the calculated tolerance factor and experimental lattice parameters of $Ba_{0.8}Sr_{0.2}Ce_{0.9-x}Zr_xY_{0.1}O_{3-\delta}$. Matsumoto investigated chemical stability of $BaCeO_3$-based proton conductors doping different trivalent cations with thermogravimetry (TG) analysis and depicted that stability increases with reduction in ionic size of the dopant, which correlate with the present result [23]. Also S. Wang et al. confirmed the stability of Sr doped barium cerates in wet atmospheres which are in agreement with the present result [21].

Scanning Electron Microscope and EDAX Analysis

Fig 3 shows the surface morphologies of the sintered $Ba_{0.8}Sr_{0.2}Ce_{0.9-x}Zr_xY_{0.1}O_{3-\delta}$ pellet powders. The

ceramic pellets are well dense although very few pores are noticed which may be due to shrinkage in the oxide volume that aroused from the surface water and residual organics during high temperature treatment. The powders prepared from citrate EDTA sol- gel process had a dense and uniform grain size average value ranging from 1.83 to 3.18 µm from x=0.04 to x=0.2.

A slight increase in the grain size is observed as Zr doping increased. So this composition with good sintering ability is suggested to be a promising electrolyte material for P+-SOFC applications.

The SEM and EDS spectra can be marked as a reference to detect possible BaO accumulation at grain boundaries EDX analysis confirmed the embellishment of Sr and Ce while depletion took place in barium.

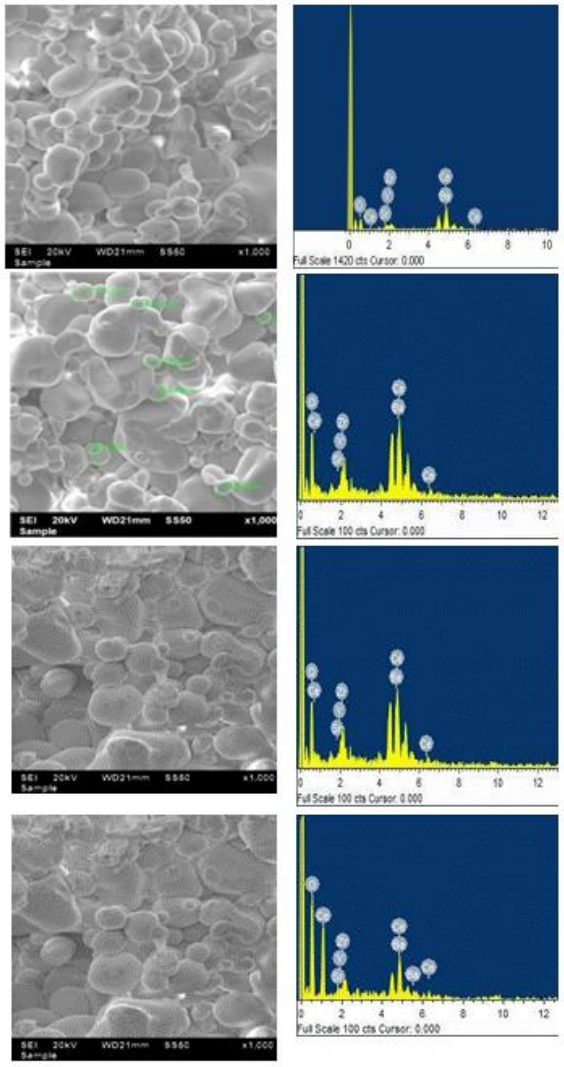

Fig 3 SEM AND EDAX spectra of samples

The bulk densities of the sintered powders are measured by the Archimedes displacement principle and theoretical density from XRD. Present EDX spectra showed that the molar ratio of (Ba + Sr) / (Ce + Zr + Y) is around 0.87 at the bulk region which is lower than the ratio of the (Ba + Sr)/ (Ce + Zr + Y) precursor =1:1.The observation of Ba deficient phase can be likely due to BaO evaporation at high sintering temperatures. The relative density of all the samples sintered at 1300°C are found to be around 89% of the theoretical density and its value can be confirmed from the SEM images. Sintering at higher temperatures may report growth in the density but there may be a chance of BaO evaporation. The idea of the present study is to measure the conductivity at low sintering temperatures**.**

Tolerance factor close to unity indicates ideal cubic structure and any deviations indicate distortions from cubic to orthorhombic (Pbnm) structure which involves rotations of Octahedral of BO_6. It is evident that there is a slight increase in the tolerance factor when Sr in doped in $BaCeO_3$ (0.8546) and the composition showed orthorhombic phase which is evident from XRD analysis.

Fourier Transform Infrared Spectroscopy

The phase purity of the formed $Ba_{0.8}Sr_{0.2}Ce_{0.9-x}Zr_xY_{0.1}O_{3-\delta}$ may be accurately identified by FTIR better than XRD because of the amorphous nature of the carbonate phase. Fig 4 represents the FTIR Spectra of the sintered samples. The peaks near 540 – 696cm^{-1} and 610-700 cm^{-1} are assigned to metal oxide Sr-O bond.The peaks near 860– 869 cm^{-1} may be assigned to the = C-H bond and the peaks shifted slightly to higher wave number side with increase in the Sr content. The strong peak near 1058 – 1078 cm^{-1} may be due to symmetric C-O stretch. The transmittance bands around 1438.9, 1447.640,1465.07cm^{-1} may be due to asymmetric C-C stretch that can be due to the chealation and polymerisation process resulting in the formation of metal complexes. The peak at 1653.119cm^{-1} is assigned to the characteristic asymmetrical split stretching of carbonate compound from CO_2 related with $Ba(NO_3)_2$ that generates $BaCO_3$ and the peak at 1751.131 cm^{-1} may be assigned to C=O stretch [25]. All the samples exhibited a similar spectrum with a carbonate peak near 1700 cm^{-1}. The C-O bonding region is the indication of presence of organic content in the residual oxides. The small band

at 2400cm^{-1} in the calcined sample of composition x=0.04 may be due to entrapped atmospheric CO_2

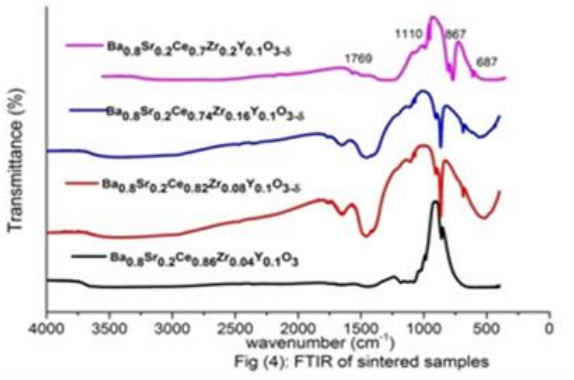

Fig (4): FTIR of sintered samples

3.6 Raman Spectroscopy

A Raman mapping technique is applied to study the local phase distribution of the Ba0.8S0.2Ce0.9-xZrxY0.1O$_{3-\delta}$ oxides in this study Fig 5. The small peak seen in the range 100 cm-1 might be assigned to the stretching mode of the carbonate ion around the Sr ion. The Raman band around 366 cm-1 are SrCeO3 like and 461.5 cm-1 are ZrCeO2 like second phase which may be attributed as the bending modes of ZrO6 [26- 28]. The bands in the region between 542-565 cm-1 might be attributed to the stretching mode of oxygen ion around strontium. The peaks between1490-1520 cm-1 may be due to SrCO3 which may be due to decrease of the effective atomic mass. This is consistent with XRD that CeO2 like second phase diminishes with increase in Zr content.

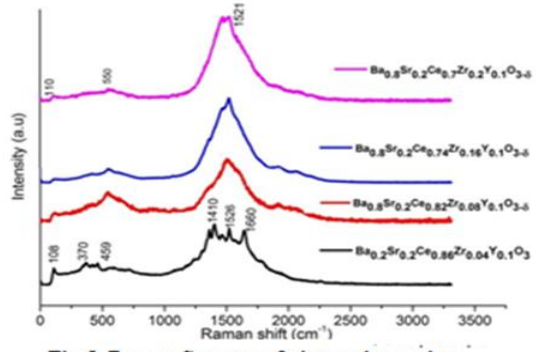

Fig 5. Raman Spectra of sintered samples

Impedance measurements

Electrolyte conduction greatly has an impact on the overall energy performance of high temperature solid oxide fuel cells. Here the ionic conductivity of the $Ba_{0.8}Sr_{0.2}Ce_{0.9-x}Zr_xY_{0.1}O_{3-\delta}$ is calculated as a function of temperature in air atmosphere with 3% relative humidity. The impedance spectra are plotted from room temperature to 500°C. The temperature is limited to 500°C due to instrumental confinement and measurements at higher temperature are under process which will be further reported further. The spectra comprises of 3 arcs at low, high and medium frequencies corresponding to the interior of grain, grain boundary and the electrode respectively [29]. In the Nyquist plots of the present work as reported from Fig 6, the high frequency and low frequency arcs are not observed due to the instrumental limitations of temperature. Hence the bulk response is unfolded to the high frequency intercept of the medium arc with the real axis which portrayed variations of about two to three orders of magnitude with rise in temperature from 30 to 500°C.The semi circular pattern represents the electrical process taking place that can be represented in an electrical circuit with a parallel combination of resistive and capacitive elements.

Ac conductivity studies

The Ac conductivity is calculated from dielectric data using the relation (7).

$$\sigma_{AC} = \omega \varepsilon_r \varepsilon_0 \tan\sigma \quad (7)$$

The kind of temperature dependence of Ac conductivity testify that the conduction in the material is a thermally activated process in which the motion of oxygen vacancies initiates activation energy.

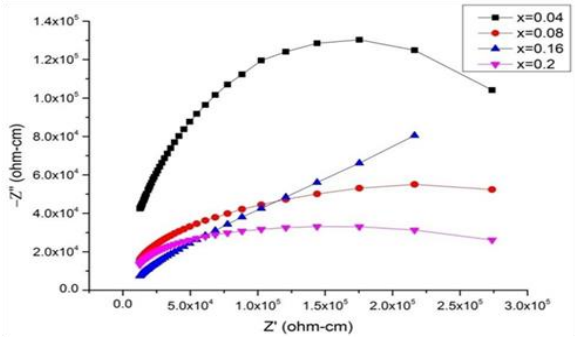

Fig 6: Nyquist plots of the sintered samples.

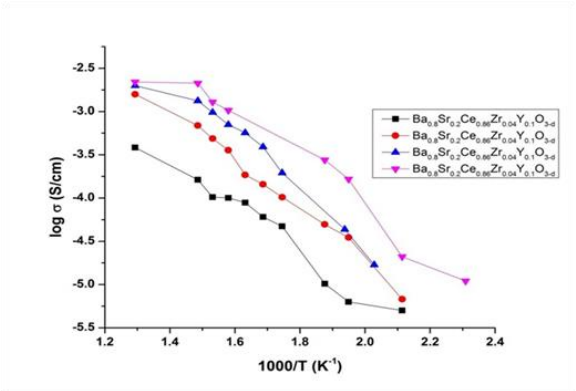

Fig 7: conductivity Vs temperature graph of the sintered samples

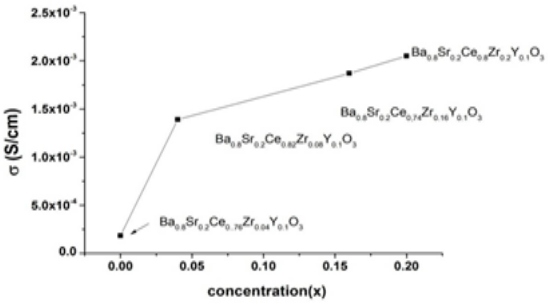

Fig 8: Temperature Vs Concentration graph of the sintered samples

The Arrhenius plots calculated from the conductivity data in the dry and wet air atmosphere of all the samples followed a linear trend as show in the Fig 7. Conduction of oxygen ions takes place with the help of oxygen vacancies present in the lattice. The conductivity in dry air does not delineate any sign of proton conduction due to absence of water to create the protonic charge carries. Hence a low conductivity value is reported in humid atmosphere but the present compound exhibited a comparable value because of its synthesis process of Citrate precursor sol-gel which resulted in more conductivity at less sintering temperature with increased density. The protonic conductivity of BCZY film in air filled with moisture was 0.83 x 10^{-3} S/cm at 400°C synthesized by spray pyrolysis deposition mechanism given by Yuji Okoyama [26, 27]. The rise in conductivity due to Zr incorporation may be also due to removal of CeO_2 like or $ZrCeYO_2$ like second phase which is agreement with FTIR and Raman measurements [13]. Among the samples, the composition with Zr content 0.2 reported highest conductivity which is in agreement with the previous measured values. A comparison of activation energy along with conductivity of the samples with other reported literature is presented in Table 2. In ABO_3 perovskite presence of oxygen vacancies result in the formation of protonic defects due to dissociative absorption of water as indicated by KrÖger-Vink notion**.** The formation of hydroxyl ions with oxygen vacancies instigate on the oxygen ion site for the incorporation of water through the reaction given below.

$$H_2O + V_o + O_o^x \Leftrightarrow 2OH_o \quad (9)$$

The mechanism of proton migration followed by series of jumps from one position to another is suggested by Iwahara [5] and further experimented by Kreuer [4].In the presence of hydrogen, hydrogen feasibly reacts with oxide ions in the lattice producing electrons and hydroxyl groups given by the reaction

$$\frac{1}{2}H_2 + O_o^x = OH_o + e^{l} \quad (10)$$

Oxygen vacancies are treated as the main defects at high temperatures. The activation energy of the sample with Zr content x=0.04 to 0.2 (0.2-0.37eV) is calculated from the slope of the plot Log σ *vs.* 1000/T which is found to be below than that of the reported value available in literature [15, 29].

The conductivity values of $Ba_{0.8}Sr_{0.2}Ce_{0.9-x}Zr_xY_{0.1}O_{3-\delta}$ is reported to be 2.05x10^{-3} S/cm and the conductivity depicted an enormous hike with rise in temperature from ~10^{-5}S/cm at room temperature to ~10^{-3}S/cm above 300°C. In the present composition as trivalent Y^{3+} is replaced with Ce^{4+}, oxygen vacancies are created which in turn trap protons that make defect pairs that aid in the formation of electric dipoles [31, 32]. The increase in conductivity with hike in temperature reveals that this composition exhibits ionic conduction. With increase in the concentration of Zr, the grain size increased. As the grains grew larger it resulted in less grain boundary which is favours decrease in grain boundary resistance. As expected Yttrium, strontium and Zirconium codoping simultaneously into the lattice hiked the conductivity values and hence this composition can be considered as a promising electrolyte if all the values like sintering temperature and time are proportionally controlled

Table 2. Comparison of the grain conductivity (σ_g) and activation energy (E_a) with the reported values

Compound	Sintering Temperature	σ_g (S/cm)	E_a (eV)	Ref.
BaZr0.1Ce0.7Y0.1Yb0.1O3-δ	1600°C/4hrs	0.018 (550°C /wet O_2)		[33]
Ba0.8Sr0.2Ce0.8Zr0.2Y0.2O3- δ	1600°C/4hrs	0.009 (800°C air/ 3% rel humidity)		[13]
Ba0.6Sr0.4Ce0.6Zr0.4Y0.2O3- δ	1600°C/4hrs	0.010 (800°C air/ 3% rel humidity)		[9]

$Ba_{0.8}Sr_{0.2}Ce_{0.65}Zr_{0.25}Y_{0.1}O_{3-\delta}$	1300°C/5hrs	0.007 (800°C air/3% rel humidity) $0.83x10^{-3}$ (400°C /moist air)		[35]
$Ba_{0.04}Ce_{0.96}Zr_{0.04}Y_{0..2}O_{3-\delta}$	1100°C/5hrs			[34]
$Ba_{0.8}Sr_{0.2}Ce_{0..86}Zr_{0.04}Y_{0..1}O_{3-\delta}$	1300°C /5hrs	$8x10^{-4}$ (500°C wet air)	0.42	This work
$Ba_{0.8}Sr_{0.2}Ce_{0.82}Zr_{0.08}Y_{0.1}O_{3-\delta}$	1300°C/5hrs	$1.389x10^{-3}$ (500°C wet air)	0.39	This work
$Ba_{0.8}Sr_{0.2}Ce_{0.74}Zr_{0.16}Y_{0.1}O_{3-\delta}$	1300°C/5hrs	$1.87x10^{-3}$(500°C wet air)	0.38	This work
$Ba_{0.8}Sr_{0.2}Ce_{0.7}Zr_{0.2}Y_{0.1}O_{3-\delta}$	1300°C/5hrs	$2.05x10^{-3}$(500°C wet air)	0.37	This work

CONCLUSIONS

This study systematically explained the relationship between Zr doping content and microstructure, Chemical stability and conductivity of $Ba_{0.8}Sr_{0.2}Ce_{0.65}Zr_{0.25}Y_{0.1}O_{3-\square}$ ($0 \leq x \leq 0.25$) electrolyte synthesized by Sol-Gel method. Single phase perovskite nanostructured $Ba_{0.8}Sr_{0.2}Ce_{0.65}Zr_{0.25}Y_{0.1}O_{3-\square}$ powders are obtained by a modified sol-Gel pechini process. The lattice constants and unit cell volumes are found to reduce as Sr atomic percentage increased in accordance with the law of Vegard, confirming the formation of Solid Solution. Incorporation of Zr into the composition enhanced grain growth besides suppressing the formation of $ZrCeO_2$ like second phase. Among the synthesized samples $Ba_{0.8}Sr_{0.2}Ce_{0.7}Zr_{0.2}Y_{0.1}O_{3-\square}$ pellet with orthorhombic structure showed highest conductivity with a value $2.05x\ 10^{-3}$ S/cm(wet air with 3% relative humidity) at 50°C due to its smaller lattice volume, bigger grain size and lower activation energy that led to excessive increase in conductivity. All pellets exhibited good chemical stability when exposed to air and H_2O atmospheres. Comparisons with the literature showed the importance of the method of synthesis on the properties of the present synthesized powders. This study elucidates that $Ba_{0.8}Sr_{0.2}Ce_{0.9-x}Zr_xY_{0.1}O_{3-\square}$ composition will be a promising electrolyte for use as an electrolyte in SOFC.

ACKNOWLEDGEMENTS

The authors wish to thank the Coordinator DST-Purse Programme, Advanced Analytical laboratory, Andhra University for providing XRD, SEM, FTIR and LCR measurements used in this work.

REFERENCES

[1] Atkinson A, Barnett S, Gorte R J, Irvine J T S, M C Envoy A J, Mogensen M, Singhal SC, Vohs J (2004) *Nature Mater* 3:17. Doi:10.1038/nmat 1040

[2] Shao Z, Haile S M (2004) *Nature* 431:170.doi:10.1038/nature02863

[3] Brain CH, *Steele and Angelika Heinzel* (2001)**.**Nature 414:345.doi:10.1038/35104620

[4] Kreuer K D (2003) Mater-Res 33:333.doi:10.1146/annurev.matsci.33.022802.0 91825

[5] Iwahara H, Asakura Y, Katahira K, Tanaka M (2004) Solid State Ionics 168:299

[6] Xie K, Yanb R Q, Liua X Q (2009) $BaCe_{0.7}Ti_{0.2}Y_{0.2}O_{3-\square}$. J Alloys Comp 479:40-2

[7] Hung I M, Peng H W, Zheng S L, Len C P, Wu J S (2009). J Power Sources 193:155-9

[8] Bi L, Zhang SQ, Zhang L, Tao ZT, Wang H Q, Liu W (2009) Int J Hydrogen Energy. 34(5):2421-5.

[9] Sheng-Wei Lee, Chung-Jen Tseng, Jeng-Kuei Chang, Kan-Rong Lee, Chia-Tzu Chen, I-Ming Hung, Sheng-Long Lee, Jing-Chie Lin (2014). Journal of Alloys and Compounds 586 : 506-510.doi:10.1016/j.allcom.2013.101

[10] Gong M, Liu X, Trembly J P, Johnson C (2007). J Power Sources 168:289-98

[11] Zhong Z M (2007) Solid State Ionics 178:213-20.

[12] Lu J D, Wang L, Fan L H, Li H, Dai L Guo H X (2008). J. Rare Earth 26: 505-510

[13] Kan-Rong Lee, Chung-Jen Tseng , Jeng - Kuei Chang, I-Ming Hung, Jing-Chin, Sheng-Wei Lee (2013). International Journal of Hydrogen Energy 38:11097-11103

[14] Ryu K H, Haile S M (1999). Solid State Ionics 125: 355-367.

[15] Amini MM, Mirzaee M (2009). Ceram Int 35:2367–2372

[16] P.Babilo, Udo T, Haile S M (2007) J. Mater. Res. 22:1322-1330

[17] Cetvera R B, Oyama Y,Yamaguchi S (2007). Solid state Ionics 178 569-574

[18] H.P. Ding, B. Lin, X Xue, X. Liu, G.Y. Meng (2010) J.Power Sources 195:3 775-778.

[19] Scholten M J, Schoonman J, Van Miltenberg J C, Oonk H A J (1993Solid State Ionics 61:83
[20] Fanglin Chen, Toft Sorensen O, et.al. (1997). J .Mater. Chem. 7:481-485
[21] S Wang, F Zhao, L Zhang, K Brinkman, F Chen (2010) J of compd and alloys 506 (2010) 263-267.doi:10.1016/j.jalcom.2010.06.188
[22] Bonanos, K.S. Knight, B. Ellis, (1995) Solid State Ionics 79 (1995) 161-170.
[23] Matsumoto H, Kawasaki Y, et.al (2007) Electrochemical and Solid State Letters 10 4.
[24] LU Jingde et.al. (2007) Journal of Rare Earths (2008) 26 4 504-510.
[25] Nafisah Osman, Najwa Adni Ibrahim, Mohid, AzLan Mohd, Oskar Hasdinor Hassan (2014) Sains Malaysia 43:9 :1373-1378
[26] Long R Q,Haung Y P,Wan H L (1997) J. Raman SpectroSc 28: 29-32
[27] Yuji Okoyama,Kaori Isa, Young Sung Lee, Takaaki Sakai (2015) . Solid State Ionics 275:35-38
[28] Kim B K, Hamaguchi H O (1997) *Mode assignments of the Raman spectrum of monoclinic zircoina by isotropic exchange technique*. Phys Stat Sol B 203:557-563.
[29] Haile S M, Staneff G, Ryu K H (2001). Journal of Materials Science 36 5:1449-1160
[30] K. D. Krekuer, (1997) *Solid State Ion* 97 :1-15.
[31] Y.Yamazaki, R. Hernandz –Sanchez, S.M Haile (2010). J Mater Chem 81 58-66.
[32] Kjolseth C, Fjeld H, et.al. (2010) *Solid State Ion.* 181:268-275.doi:10.1016/j.ssi.200.01.014.
[33] D. K. Lim, C. J. Park, et.al (2010). *Int J of hydrogen energy* 35:10624-10629.
[34] Dubal S U, Jamale A P, bhosale C H, Jadhav L D (2015) *Applied Surface Science* 324: 871-876.doi 10.1016/j.apsusc.2014.11.063.
[35] Simona Barison, Batlagliarin M, Tommaso Cavallin, Lioudmila Doubova, Monica Fabrizio, Cecilia Mortalò, Stefano Boldrini, Lorenzo Malavasi and Rosalba Gerbasi (2008) J. Mater. chem 18:5120-5128.doi:10.1039/B817275.
[36] Madhuri Sailaja J et.al (2016) journal of Asian Ceramic Societies. 10.1016/J. Jascer 2016.12.004